ACS APPLIED MATERIALS & INTERFACES

Research Article

www.acsami.org

# Wicking Nanopillar Arrays with Dual Roughness for Selective Transport and Fluorescence Measurements

Jennifer J. Charlton,[†,‡] Nickolay Lavrik,[*,§] James A. Bradshaw,[‡,†] and Michael J. Sepaniak[*,†]

[†]The University of Tennessee Knoxville, Department of Chemistry, Knoxville, Tennessee 37996, United States

[‡]Y-12 National Security Complex, Analytical Chemistry Organization, Oak Ridge, Tennessee 37830, United States

[§]The Center for Nanophase Material Sciences, Oak Ridge National Laboratory, Oak Ridge, Tennessee 37830, United States

Supporting Information

**ABSTRACT:** Silicon nanopillars are important building elements for innovative nanoscale systems with unique optical, wetting, and chemical separation functionalities. However, technologies for creating expansive pillars arrays on the submicron scale are often complex and with practical time, cost, and method limitations. Herein we demonstrate the rapid fabrication of nanopillar arrays using the thermal dewetting of Pt films with thicknesses in the range from 5 to 19 nm followed by anisotropic reactive ion etching (RIE) of the substrate materials. A second level of roughness on the sub-30 nm scale is added by overcoating the silicon nanopillars with a conformal layer of porous silicon oxide (PSO) using room temperature plasma enhanced chemical vapor deposition (PECVD). This technique produced environmentally conscious, economically feasible, expansive nanopillar arrays with a production pathway scalable to industrial demands. The arrays were systematically analyzed for size, density, and variability of the pillar dimensions. We show that these stochastic arrays exhibit rapid wicking of various fluids and, when functionalized with a physiosorbed layer of silicone oil, act as a superhydrophobic surface. We also demonstrate high brightness fluorescence and selective transport of model dye compounds on surfaces of the implemented nanopillar arrays with two-tier roughness. The demonstrated combination of functionalities creates a platform with attributes inherently important for advanced separations and chemical analysis.

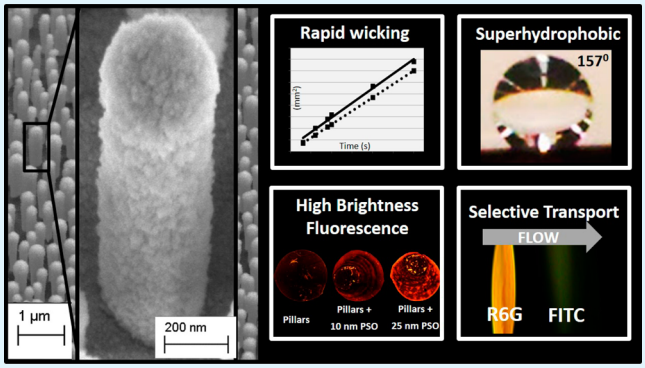


**KEYWORDS:** *nanopillars, porous silicon oxide, superhydrophobic, enhanced fluorescence, capillary flow wicking, selective transport*

## INTRODUCTION

There is a strong demand for high sensitivity platforms for the fluorescence detection of low level and/or low quantum yield samples. Some traditional approaches that can increase the effectiveness of a fluorescence analysis include increasing the intensity of the excitation field and emission collection efficiency, effectively transporting, and concentrating an analyte within the area to be analyzed, and isolating from interfering species.[1] Herein, we fabricate and offer a convenient means to optimize, a single multifunctional platform that combines all of these approaches with an emphasis on tailoring nanoscale features. Using silicon nanopillars with vertical sidewall profiles and adding second level roughness via a porous silicon oxide (PSO) coating, we study attributes including wicking, superhydrophobicity, fluorescent brightness, and selective transport that are beneficial in creating a platform for low level fluorescence analysis. Our specific approaches and designs were driven by two main considerations. First, a unique combination of wicking dynamics and superhydrophobicity of these nanostructured surfaces can lead to capillary assisted selective transport, concentration,[2,3] and delivery[4−6] of minute quantities of low level samples. Second, appropriately designed silicon nanopillars are known to facilitate enhancement[7,8] and collection of fluorescence signals.[9] The use of micro- and nanoscale pillar arrays have garnished significant attention as a platform for separations in pressure driven microfluidic systems[4,5,10,11] and systems that use electrophoretic pumping.[12] Because of their high surface area and wicking properties[13] pillar arrays are also promising as a platform for capillary driven microfluidic systems that take advantage of the open capillary architecture. When applied to analytical separations, such "open channel" microfluidic systems are anticipated to possess many advantages including the potential for multiplexing separations, capability of orthogonal separation formats, imaging separations without rigorous temporal limitations, as well as the overall simplicity often associated with planar chromatography.[6] These advantages combined with the low sample consumption common to micro and nanofluidic systems open the door to

Received: July 14, 2014
Accepted: September 23, 2014
Published: September 23, 2014

  

a platform for point-of-care analysis of traditionally difficult and high value samples.[14−17] Many current point-of-care capillary driven devices, such as lateral flow (immuno)assays, use a transport medium of nitrocellulose with pore sizes ranging from 0.05 to about 12 $\mu$m that can vary depending on manufacturing and storage conditions (including temperature and humidity). These poorly controlled changes in porosity alter flow dynamics of the substrate and can make it challenging to realize conditions that facilitate transport and allow an optimal reaction time for analysis.[18] Therefore, the main motivation behind the present study is to identify new types of wicking substrates that are free from environmentally induced changes in porosity, wetting, and capillary transport properties and also deterministically tunable as well as practically reproducible.

The remarkably diverse wetting phenomena observed on micro and nano fabricated surface textures[13] range from directional wicking and superwicking[19−31] to superhydrophobicity and omni-phobicity.[23,28,30,32] Among various classes of previously explored surface nanostructures and nanotextures, silicon pillar arrays have been of our particular attention since they have the potential to combine the unique wetting properties associated with forests of small diameter pillars,[33] as well as unique optical properties associated with optical field enhancements in vicinity of nanoscale cylindrical dielectric resonators.[7−9] In particular, it has been recently shown that resonance enhancement of optical fields on the surface of silicon nanopillars facilitates detection of a small number of fluorescently labeled biological molecules.[8] Arrays of high aspect ratio nanopillars made from materials other than silicon can also provide nonresonance increases in fluorescence brightness and, respectively, improved figures of merit in fluorescence based analytical techniques due to a geometric factor, that is, substantially increased surface areas.[34] Furthermore, the superhydrophobic properties of pillar arrays can be useful in delivering minute quantities of analytes while overcoming fundamental limitations of more conventional systems when diffusion limited kinetics slows down transport of highly dilute chemical species in ultralow volumes.[2]

Both the optical resonances[7,8] and the fluid dynamics[33] observed in silicon pillar arrays can be tailored by changing the pillar size, shape, and density. To date, methods to reproducibly fabricate pillars with sub micrometer diameters often involve complex advanced lithography methods[7,8,35] or surface assembly of nanoparticles.[36] While several methods can produce highly ordered arrays of silicon pillars with diameters in the 100−500 nm range, most have practical limitations. Electron beam lithography (EBL) is often used to fabricate precisely defined pillar arrays with diameters around 100 nm.[8] The EBL approach requires expensive equipment and is a slow serial process, creating practical limits as to the size and quantity of fabricated arrays. On the other hand, the bottom up approaches such as surface assembly of nanoparticles have the ability to quickly cover large areas creating etch masks suitable for subsequent fabrication of tightly spaced pillar arrays.[36,37] However, these methods lack the ability to reproducibly create variations in the pillar size within the same wafer. Moreover, the use of nanoparticles is of a potential concern because environmental nanopollutants can pose serious health risks.[38]

In the present study, we show that the challenge of creating expansive arrays of silicon nanopillars with average diameters tunable from 100 to 500 nm can be addressed very efficiently through the thermal dewetting of thin Pt films followed by anisotropic reactive ion etching (RIE) of silicon oxide and silicon. Aiming to create substrates with a combination of high surface area and other functionalities important in planar chromatography and trace level analytical fluorescence analysis, we explore room temperature plasma enhanced chemical vapor deposition (PECVD) which allowed us to overcoat the silicon nanopillar arrays with a conformal layer of porous silicon oxide (PSO) and prepare wicking substrates with two-tier roughness.

## MATERIALS AND METHODS

To create arrays of approximately circular patterns, we utilized thermally induced dewetting of thin Pt films deposited on silicon surfaces with a thermally grown silicon dioxide ($SiO_2$). Nanopillar arrays were formed due to the masking role of Pt islands during reactive ion etching of $SiO_2$ and silicon as described in our previous work.[39] Subsequently, we analyzed average diameter, standard deviation, average spacing and density of pillars formed on the silicon wafer that had Pt film with original thickness varying from 5 to 19 nm. Finally, we create a secondary level of nanoscale roughness through the deposition of a PSO layer on the pillar surface using room temperature PECVD[40−42] and observe the effects this process has on the wicking of silicone oil. Experimentally determined wicking rates of silicone oil and ethanol were also compared to the results to an analytical model developed by Mia et al.[35] based on a widely accepted rough wetting model.[44]

Post-silicone-oil-treatment, it is observed that we created a hydrophobic surface with high fluorescent brightness and chemical selectivity with the aim of developing an analytical platform.

**Pillar Fabrication.** As shown in Figure 1, our fabrication sequence started with physical vapor deposition of a Pt film (Thermonics Laboratory, VE-240) on a p-type silicon wafer with 100 nm of thermally grown $SiO_2$. During the Pt deposition, the deposition rate and the average (mass based) thickness of the deposited metal were monitored with a quartz crystal microbalance while a shutter that

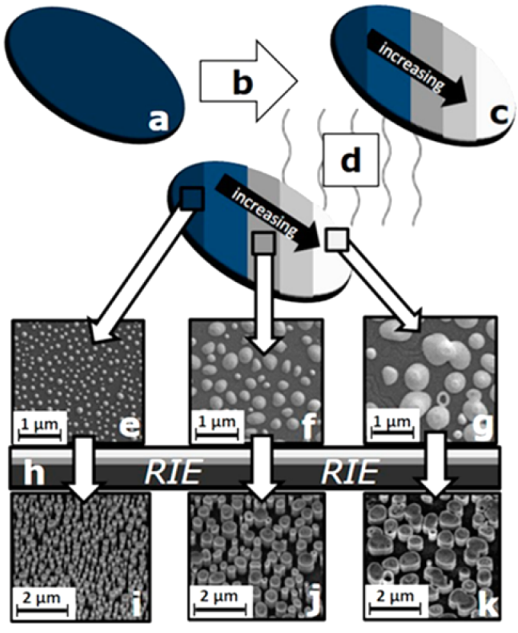


**Figure 1.** Process sequence used to fabricate silicon pillar arrays in present work. (a) A silicon wafer with 100 nm of thermally grown $SiO_2$ is used as a starting material. (b) Physical vapor deposition of Pt results in regions (c) with varying Pt thicknesses across wafer. (d) Thermal processing in a mixture of argon and hydrogen yields Pt islands. SEM of Pt islands from (e) 5, (f) 10, and (g) 17 nm films acting as a mask during subsequent (h) RIE of silicon. SEM of pillar arrays with various morphologies formed after RIE form (i) 5, (j) 10, and (k) 17 nm Pt films.

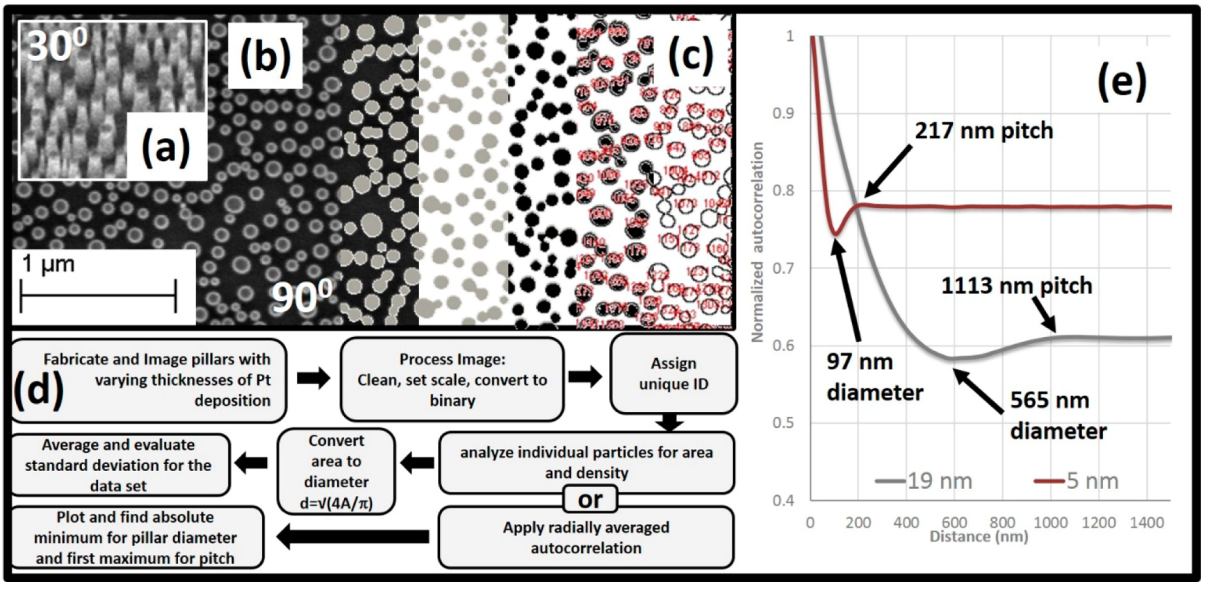


**Figure 2.** (a) SEM image of a silicon pillar array taken at 30° angle. (b) Top view SEM images of a similar array and a sequence of graphics produced from the digital image processing, (c) areas with assigned unique ID, (d) flow diagram of analysis of image to characterize pillar size, dispersity, and density, and (e) example plots of radially averaged autocorrelation of the pillars from 5 and 19 nm Pt deposition with pitch and diameter clearly shown.

separated the metal source and the substrate acted as a mask. This mask was incrementally moved across the silicon wafer in such a way that Pt thickness varied in 1 nm increments from 5 to 19 nm across the four inch silicon wafer. As a result, as series of distinct 5 mm wide regions for each average thickness of Pt was created on a single wafer. The platinum film was then thermally annealed in a 10:1 mixture of argon and hydrogen at 735 Torr in a cold wall furnace (Easy Tube 3000, First Nano, Ronkonkoma, NY) equipped by a radiative heat source. During the anneal step the heat source was set to its maximum power (22 kW) for 8 s yielding an estimated maximum substrate temperature of 900 °C. The thermally induced metal film dewetting created circular masking patterns (see Figure 1e). These platinum islands were subsequently used as a selective mask for anisotropic reactive ion etching (Oxford PlasmaLab, Oxford Instruments, UK) of the substrate material as described previously.[39] The resulting 1 ± 0.2 $\mu$m tall silicon pillars with the remaining Pt caps are similar to those created via EBL patterning and used as a platform for enhanced fluorescence analysis in our previous work.[7,8] However, the pillars that are over coated with the PSO have a conformal material surface.

**PSO.** With the goal of increased surface area we added a second level of roughness to the sidewalls, floors, and tops of our pillared substrates via a room temperature PECVD (PECVD, Oxford Instruments) of PSO.[41,42] During the deposition of PSO the substrate temperature and chamber pressure were 27 °C and 600 mTorr, respectively. The capacitively coupled RF plasma source was set to a power of 150 W. The gas flow rates of 5% $SiH_4$ in Ar and $N_2O$ were 75.0 and 600 sccm, respectively. Pillar arrays with two thicknesses of PSO coating were prepared and subsequently evaluated against the arrays without PSO.

**Pillar Characterization.** The fabricated pillar arrays were imaged using scanning electron microscopy (SEM) (Carl Zeiss Merlin, operated at 3 kV). The images were cleaned of image noise by despeckling and removing outliers less than or equal to 4 pixels. The cleaned digital images were converted to binary and analyzed for particle density and size using public domain software ImageJ 1.47 V (Wayne Rashband, National Institutes of Health, USA, see Figure 2). Although we recognize that Pt islands did not exhibit a perfect circular form, the following assumption of circular shapes gives a reasonable approximation for calculating pillar diameters

$$d = \sqrt{\frac{4A_p}{\pi}} \quad (1)$$

where $d$ is the diameter and $A_p$ is the area that was generated for the particle. Using eq 1, we calculated average pillar diameters, as well as the standard deviation and range for the pillar diameters.. Additionally, we found average pitches and validated the average diameters using the radially averaged autocorrelation. The curves shown in Figure 2e are calculated from the pair correlation of pixels of a binary image as a function of their radial distance. The absolute minimum gives pillar diameter information. The first maxima or plateau after the absolute minimum gives pillar spacing information.[43] These geometrical parameters were calculated for each of the experimental samples prepared and characterized in the present study (see Figure 2).

**Functionality Studies.** The wicking behavior was studied with the pillar arrays inserted vertically into a pool of the liquid, in an open container for the silicone oil and in a sealed vial for the ethanol (190 proof, Decon Laboratories, Inc.). The wicking progress was captured with a 5.0 MP autofocus camera with LED Flash (LG Optimus F3) at known times. Using ImageJ software the digital images were scaled based on a known dimension and the z (displacement of the wicking front) was measured from the surface of the wicking liquid to the visible wicking front. Initially, silicone oil (HIVAC F4) was applied and allowed to wick at room temperature until the full wafer was covered the baked at 100 °C for 72 h. Subsequently, excess oil was removed in a five part wash using successive rinses of ethanol, toluene (Fisher Scientific), THF (Fisher Scientific) 90% then THF 10% with 18 MΩ deionized water, and finally 18 MΩ deionized water. The substrates rendered hydrophobic after this process were used to study the wicking dynamics of ethanol. The contact angles were found by depositing 2.5 $\mu$L of 18 MΩ deionized water on each substrate, and subsequently imaging the drops with the aforementioned camera at 90° from substrate surface. The angle was visually measured by a digitally overlaid protractor. Fluorescence brightness was evaluated by analyzing fluorescence images of the substrates spotted with 2.5 $\mu$L drop of $1 \times 10^{-10}$ M rhodamine 6G in a 90% water: 10% ethanol solution. Fluorescence images were obtained with a 30 s collection time, a 510−560 nm excitation source and a camera gain of 1.5 (Nikon Ellipse E600 Fluorescence Microscope). For the selective transport analysis, pillars with 96 nm average diameter were overcoated with 25 nm of PSO and spotted with a 1 $\mu$L drop of a mixed $1 \times 10^{-7}$ M rhodamine 6G and $1 \times 10^{-7}$ M fluorescein isothiocyanate (FTIC) in

10% ethanol 90% water and allowed to dry for 48 h. The spotted array was inserted perpendicular to just below the visible spot into 30% water 70% ethanol solution in a sealed vial and allowed to wick 1 cm past the original spot. The array was immediately removed from the vial and imaged with Nikon Eclipse LV150 microscope using the 5× objective. The microscope was equipped with a halogen lamp light source, a multicolor fluorescence cube (DAPI-FITC-TRITC), and a color CCD camera (DS-2M, Nikon, Inc.) controlled by NIS-Elements software. Fluorescence color (RGB) images with 16-bit color depth per channel were acquired by integrating a sequence of four 8-bit color images.

*Surface Analysis.* A flat silicon substrate was submerged in silicone oil and baked with a control sample that was not exposed to oil at 100 °C for 72 h. The samples were rinsed in various solvents and evaluated via ellipsometry to evaluate their effects on the thickness of the physiosorbed layer of silicon oil. The solvents included the five part (ethanol, toluene, THF, 90 THF/10 $H_2O$, $H_2O$) rinse described previously, acetone, methylene chloride, and trichloroethylene by submerging sample in clean solvent 1 min repeated three times. Additionally the samples were soaked in water and ethanol for 1 and 24 h. Ellipsometry was carried at 70° incidence and 635 nm probing wavelength using a UVISEL spectroscopic ellipsometer (Horiba–Jobin Yvon) with the elliptical probing area of 1 mm × 1.5 mm. Ellipsometry data were fitted to a two layer optical model using DeltaPsi2 Software (Horiba Scientific). The model included a silicon substrate, a native oxide, and an organic layer. Optical properties of silicon and silicon dioxide were taken from the DeltaPsi2 material database. We assumed a constant refractive index $n$ = 1.4 for the organic layer.

## RESULTS AND DISCUSSION

**Pillar Array Morphology.** Lee and Kim[45] have shown that surface morphologies of patterns formed as a result of Pt film thermal dewetting, and subsequently used for etching GaN nanostructures, depend on the Pt thickness as well as anneal temperature. More recently, our group has adopted a similar method to fabricate stochastically arranged silicon nanopillars with a relatively small size dispersity.[39,46] While a single thickness of Pt film[39] was annealed and used as a mask in our previous work, here we explore a range of Pt thicknesses and analyze respective pillar morphologies. Under the given annealing conditions, dewetting of Pt films thinner than 5 nm resulted in circular masking patterns that were too small to produce the targeted 1 $\mu$m tall pillars with sufficient mechanical strength. On the other hand, annealing of Pt films thicker than 19 nm led to spinodal dewetting morphologies. At the lower end of the Pt film thickness (5 nm) the average diameter of pillars is 97 nm with a %RSD of 27% and a range from 40 to 277 nm. A nearly linear increase in average pillar diameters with the increased Pt thickness is observed. This trend terminates at the higher end of the Pt film thickness (19 nm) with average diameter of 565 nm, a %RSD of 55%, and a range from 40 to 2190 nm. The average pillar-to-pillar distance (pitch) also increases with the diameter increase (Figure 3b). The pillar fractional coverage is near 50% over nearly the entire range pillar diameters decreasing to approximately 30% at the smaller diameters (Figure 3c).

**Wicking Rate.** To evaluate the role the random arrangement of the pillars plays in effecting wicking velocity, our experimentally determined results were compared with wicking velocities predicted by an analytical model for a perfectly ordered pillar arrays. This model is based on averaged geometrical parameters derived through the analysis of the fabricated substrate, experimentally measured solvent–substrate contact angles, and accepted literature values of solvent viscosity and surface tension. Modeled results were compared

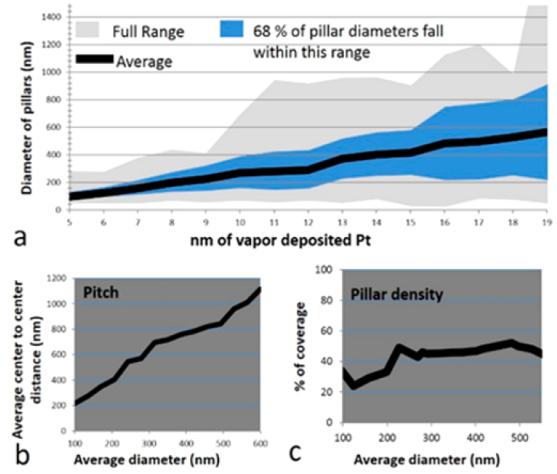


**Figure 3.** (a) Average pillar diameter and the dispersity of the diameters as a function Pt thickness. (b) The average autocorrelation calculated pillar-to-pillar distance (pitch) as a function of average pillar diameter. (c) The fractional coverage of surface occupied by pillars as a function average pillar diameter.

to the velocities experimentally observed in our system. In particular, we calculated wicking velocities for silicone oil (surface tension $\gamma$= 0.0344 N/m, viscosity $\mu$ 0.02375 Pa·s, contact angle $\theta_{oil}$ = 18°) and ethanol ($\gamma$ = 0.0224 N/m, $\mu$ = 0.00107 Pa·s, $\theta_{ethanol}$ = 22.5°) using the semiempirical model developed by Mai et al. for ordered arrays of silicon pillars.[35] The experimentally observed wicking was analyzed and compared with a previously established analytical model using the $D$ coefficient from the well-known diffusive relation

$$D = z^2/t \tag{3}$$

where $z$ is the displacement of the wicking front and $t$ refers to the time after the start of wicking.

Comparison of the experimentally determined and analytically calculated $D$ values (Figure 4) indicates slower wicking in the majority of implemented experimental systems compared to the analytical predictions for analogous perfectly ordered pillar arrays. As can be seen in Figure 4a, wicking of silicone oil in the arrays with the average pillar diameter of 97 is the only notable exception from this trend (wicking results for all arrays

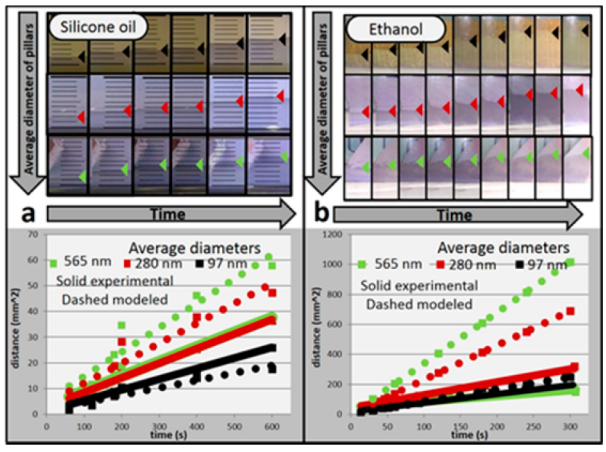


**Figure 4.** Study of the wetting behavior of (a) silicone oil and (b) ethanol on dewetted pillar arrays with average 97, 280, 565 nm diameters compared against an ordered model system.

provided in Supporting Information). We believe that this phenomenon can be explained based on the law of flow resistance in parallel channels.[47] Specifically, the model is based on a single averaged spacing motif while dewetted pillar arrays are comprised of various channel sizes on both sides of the average. With this in mind, it is reasonable to assume that the liquid flows preferentially through the path of least resistance which, in turn leads to the greater apparent wicking rate. Although nonuniform channel width is a common feature in all the samples studied here regardless of the pillar diameter, more substantial viscous losses are associated with very tall and dense arrays of pillars.[35] Therefore, a positive effect of nonuniform parallel channels on wicking velocity is likely to be much more pronounced at the lower end of the explored interpillar spacing range.

As shown in Figure 4b, the wicking behavior of the much less viscous ethanol follows a similar trend when compared to the modeled values as the silicone oil. The pillar arrays with the 97 nm averaged diameter had a slope similar to the averaged the modeled system. Mai et al.[35] reported a similar trend when wicking water in similar arrays of high aspect ratio nanopillars. They proposed that the divergence was likely due to the deformation of the mechanically weak, high aspect ratio nanopillars caused by capillary forces during the wicking process. We believe additional considerations that can have an effect on the wicking behavior between solvent systems are changes in viscosity and vapor pressure of the liquid. With the lower viscosity the high roughness of the surface does not have as large of a negative effect on the modeled wicking dynamics. Additionally the volatile nature of ethanol, combined with the extremely low fluid volumes (approximately 0.085, 0.087, and 0.093 $\mu$L per cm$^2$ for the 97, 280, and 565 nm averaged diameter systems, respectively), can permit appreciable solvent evaporation during experiments. Even a small percentage of evaporation may significantly reduce the observed displacement of the wicking front. Overall, when compared with an analytical model of the average dimensions of the system, the experimentally observed wicking dynamics of the system are affected by the randomness of the array and this effect diminishes as the %RSD of the pillar diameter decreases.

We studied the effect of a secondary roughness on the wicking dynamics of our system. As shown in Figure 5a–d, RIE pillars exhibits a mostly smooth silicon sidewall. Whereas, the pillars deposited with 10 nm of PSO shows slightly enhanced sidewall roughness, and the 25 nm thicknesss of PSO shows a greater degree of side wall roughness. With each system we evaluated the wicking behavior of both silicone oil and ethanol.

As shown in Figure 6, an increase in sidewall roughness results in a decrease in wicking velocity. Additionally, the degree to which the wicking velocity is decreased is minimized as the viscosity of the liquid decreases. We feel that these observed decreases in wicking velocity are due to additional viscous loses associated with the enhanced roughness of the pillar sidewall. These trends were observed at all average diameters (additional results found in Supporting Information).

**Superhydrophobicity.** Liquid propagation in superhydrophobic micropillar arrays is of significant interest due to unique interfacial phenomena.[31] Recent work has shown that superhydrophobic platforms can be used to concentrate droplets of dilute analyte for SERS and fluorescence detection.[2] This concentrating effect is a result of the droplet remaining in Cassie–Baxter state where the droplet maintains only contact with the tops of the pillars, leaving air underneath during an

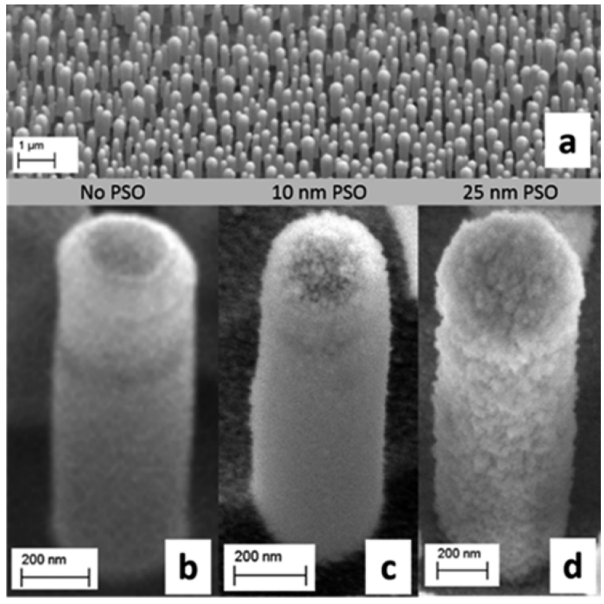


**Figure 5.** (a) Example of expansive pillar array with an average diameter of 270 and 10 nm of low temperature PECVD deposited PSO. (b) Approximately 400 nm diameter and 1500 nm tall silicon pillar (c) with 10 nm PSO and (d) with 25 nm PSO.

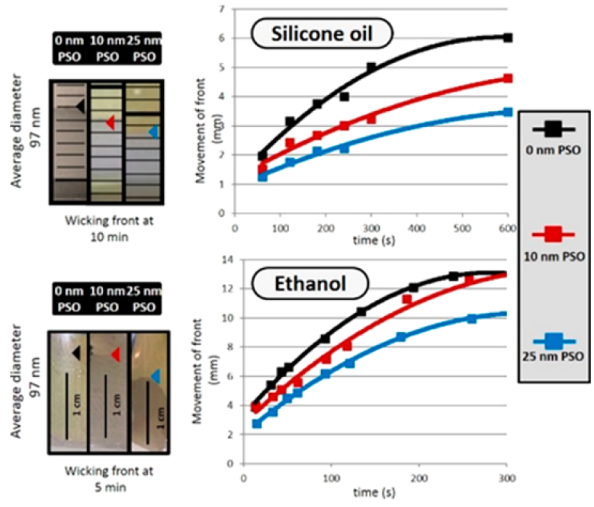


**Figure 6.** Wicking behaviors of silicone oil and ethanol on bare silicon pillar arrays and pillar arrays over coated with 10 and 25 nm PSO. Average pillar diameter in the arrays was 97 nm.

evaporative process. The point at which the energy barrier that maintains the droplet in the metastable Cassie–Baxter state and external forces reach the same order of magnitude, the transition into the Wenzel state is observed, and the droplet will penetrate the pillar array.[48] It is to be noted this evaporative concentrating effect has been shown to increase localized concentration on the magnitude of 100 fold in the spatially limited area where the Wenzel transition is observed.[3] In order for a substrate to be classified as super hydrophobic the contact angle of a water droplet must be greater than 150° and exhibit a roll-off angle less than 10°.[49] The pillar systems used in this work have a dual level roughness that is traditionally associated with superhydrophobic surfaces,[23,28−30,49] these surfaces are roughed on the microscale for one level and on the nanoscale for the second. The novelty here is that these platforms have

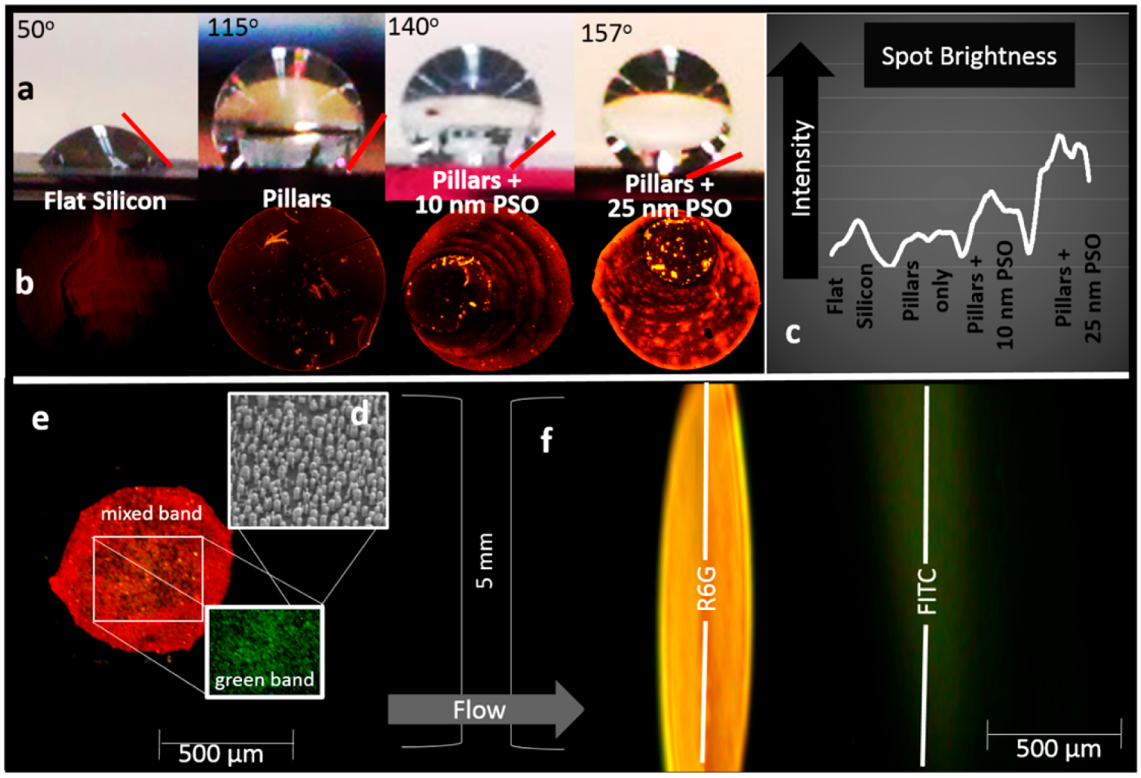


**Figure 7.** (a) Contact angle of 18 MΩ deionized water on silicone oil treated and washed flat silicon, array of silicon nanopillars with 280 nm average diameters, and similar nanopillar arrays with 10 and 25 nm of PSO-deposited on the surface, (b) fluorescent spots of $1 \times 10^{-10}$ M rhodamine 6G on each substrate, (c) fluorescence intensity for each sample, (d) SEM of dewetted pillar array, (e) FITC/rhodamine 6G mixed spot before wicking ethanol, (f) substrate showing greater selective interactions with rhodamine 6G over FITC.

both levels of roughness within the nanoscale and still maintain the greater than 150° contact angle needed to categorize them as a superhydrophobic substrate. Additionally, we chose to use a unique silicone oil based organic to functionalize the PSO-coated pillars. As it was well noted that upon wicking the silicone oil, the pillar arrays exhibited a high degree of hydrophobicity. It is reasonable to assume that a thin layer of the silicone oil led to formation of a textured surface analogous to the bioinspired self-repairing slippery surfaces (SLIPS) introduced by Wong et al.[32] When evaluating the surface with elipsometry we found that 5.5 nm of thermally grown silicon oxide was created during the curing and baking time. Upon washing with the five part rinse described previously the thickness of the oxide and organic layers were between 11 and 14 nm combined. When triple rinsing with methylene chloride the thickness was similar to the five part rinse between 11 and 14 nm. Using the harsher chlorinated solvent trichloroethylene the oxide and organic layer was reduced to between 9 and 10 nm. By contrast, with less harsh solvent systems such as acetone and extended soaks in water and ethanol the samples were very uninform and the elipsometry measurements ranged from 20 to 40 within each sample. As shown in Figure 7a, a smooth silicon surface successively exposed to the silicone oil and washed had a contact angle of 50°. However, pillar arrays with average diameters of 280 nm exposed to silicone oil exhibited a contact angle of 115°. Even higher contact angles with values approaching those characteristic of the superhydrophobic state with small contact angle hysteresis is observed only on pillars additionally modified with PSO to produce a dual level roughened surface.[28] At the secondary roughness from a 10 nm deposition of PSO the angle is 140° and at 25 nm of PSO we enter the superhydrophobic range with a 155° contact angle. The trend was similar at all of the pillar diameters.

**High Brightness.** The substrate evaluated herein was developed with the goal of creating an easily fabricated expansive platform for surface fluorescent analysis. With this in mind we tailored our synthesis based on known attributes that would create an environment to maximize the brightness of a fluorescence sample. In addition to aforementioned analyte concentration effects associated with the super hydrophobic surface, one must consider the properties of added surface area as well as optical effects associated with silicon and silicon oxide. It has been shown in previous work that silicon pillars at or near 100 nm can produce an enhanced field and subsequently an increase in fluorescent brightness over a background.[8] This enhanced field effect is tunable by pillar size allowing enhancement selective spectral signals based on wavelength.[7] Other than field effects it has been shown that fluorescence brightness can scale with increased surface area by allowing increased sample concentrations on the surface within the limited field of view of the collection platform.[34] The nanopillars as well as the PSO play an important role of adding additional surface area. Finally the highly reflective nature of $SiO_2$ can add to the increased brightness due to constructive interference of the reflected incident and fluorescence signals[9] as well as reflecting signals with an initial direction away from the collection platform a more fortuitous path toward the collecting optics. When comparing spots of similar size and concentration of rhodamine 6G, it is noted that (Figure 7b) the spot on the flat silicon and the pillars without PSO are of similar fluorescence brightness. However, high brightness of the pillars with the PSO was readily visualized and increased as the

deposition thickness of PSO increased. We used imageJ software to quantify the brightness. The average brightness of the pillars with 10 nm PSO was 2.0 times and 25 nm PSO was 3.8 times that of the pillars without the PSO. This increased brightness may be attributed to several factors. We believe the increase in brightness is caused by the increased surface area of the PSO-coated pillars, as well as the reflective nature of $SiO_2$. The increased brightness with increased PSO deposition was observed at all pillar diameters.

**Selective Transport.** The innate wicking, high brightness, and superhydrophobic properties demonstrated for the silicone oil functionalized surface of the pillar arrays with 25 nm PSO, led to testing the array for selective compound transport as fluorescence analysis is known for its broad spectral nature and the ability to isolate compounds would increase the selectivity of any method developed for use with this platform. Selective transport of compounds is based on the likely hood of chemically induced interactions of the analyte with the substrate. These interactions would allow for the selective analysis of a single compound while removing interfering species that cause increases in background fluorescence. As shown in Figure 7e, the array experienced greater selective interactions with Rhodamine with a retardation factor of 0.70 as evidenced by its lesser transport down the array. The FITC had a retardation factor of 0.82, a similar trend to traditional reverse phase TLC. This selective transport is important in the development of new platforms for open platform separations.[7]

## CONCLUSIONS

In summary, we demonstrate the straightforward processing of expansive stochastic nanoscale pillars via Pt dewetting, dry etching, and PECVD of PSO with relative ease, cost considerations, and environmental soundness. Advantages of the implemented arrays include easily tunable inter- and intrawafer average pillar diameters, dual level tunable roughness, rapid solvent wicking, superhydrophobicity, chemically selective transport, as well as the ability to promote high florescence brightness. These features, make the nanopillar arrays discussed herein, especially attractive for analytical methods and offer a pathway for the large scale production of substrates for use in separations of select compounds with florescence signal detection.

## ASSOCIATED CONTENT

### Supporting Information

Results of substrate analysis, SEM images of pillars, images and charts of wicking fronts, and wicking dynamics.This material is available free of charge via the Internet at http://pubs.acs.org.

## AUTHOR INFORMATION

### Corresponding Authors

*E-mail: lavriknv@ornl.gov.

* E-mail: msepaniak@utk.edu,.

### Notes

The authors declare no competing financial interest.

## ACKNOWLEDGMENTS

This research was conducted at the Center for Nanophase Materials Sciences, which is sponsored at Oak Ridge National Laboratory by the Scientific User Facilities Division, Office of Basic Energy Sciences, U.S. Department of Energy. This material is based on work supported in part by the National Science Foundation under Grant CHE-1144947 with the University of Tennessee. This work was supported in part by the Y-12 National Security Complex Plant Directed Research and Development fund.

## REFERENCES

(1) Demchenko, A. P. *Introduction to Fluorescence Sensing*; Springer Publishing: New York, 2009.

(2) De Angelis, F.; Gentile, F.; Mecarini, F.; Das, G.; Moretti, M.; Candeloro, P.; Coluccio, M.; Cojoc, G.; Accardo, A.; Liberale, C. Breaking the Diffusion Limit with Super-Hydrophobic Delivery of Molecules to Plasmonic Nanofocusing SERS Structures. *Nat. Photonics* **2011**, *5*, 682−687.

(3) Wallace, R.; Charlton, J.; Kirchner, T.; Lavrik, N.; Sepanaik, M. Superhydrophobic Analyte Concentration Utilizing Colloid-Pillar Array SERS Substrates. *Anal. Chem.* **2014**, in press.

(4) Lavrik, N. V.; Taylor, L. T.; Sepaniak, M. J. Nanotechnology and Chip Level Systems for Pressure Driven Liquid Chromatography and Emerging Analytical Separation Techniques: A Review. *Anal. Chim. Acta* **2011**, *694*, 6−20.

(5) Taylor, L. C.; Lavrik, N. V.; Sepaniak, M. J. High-Aspect-Ratio, Silicon Oxide-Enclosed Pillar Structures in Microfluidic Liquid Chromatography. *Anal. Chem.* **2010**, *82*, 9549−9556.

(6) Kirchner, T. B.; Hatab, N. A.; Lavrik, N. V.; Sepaniak, M. J. Highly Ordered Silicon Pillar Arrays As Platforms for Planar Chromatography. *Anal. Chem.* **2013**, *85*, 11802−11808.

(7) Wells, S. M.; Merkulov, I. A.; Kravchenko, I. I.; Lavrik, N. V.; Sepaniak, M. J. Silicon Nanopillars for Field-Enhanced Surface Spectroscopy. *ACS Nano* **2012**, *6*, 2948−2959.

(8) Kandziolka, M.; Charlton, J. J.; Kravchenko, I. I.; Bradshaw, J. A.; Merkulov, I. A.; Sepaniak, M. J.; Lavrik, N. V. Silicon Nanopillars as a Platform for Enhanced Fluorescence Analysis. *Anal. Chem.* **2013**, *85*, 9031−9038.

(9) Choudhury, B. D.; Casquel, R.; Bañuls, M. J.; Sanza, F. J.; Laguna, M. F.; Holgado, M.; Puchades, R.; Maquieira, A.; Barrios, C. A.; Anand, S. Silicon Nanopillar Arrays with SiO2 Overlayer for Biosensing Application. *Opt. Mater. Express.* **2014**, *4*, 1345−1354.

(10) De Malsche, W.; Eghbali, H.; Clicq, D.; Vangelooven, J.; Gardeniers, H.; Desmet, G. Pressure-Driven Reverse-Phase Liquid Chromatography Separations in Ordered Nonporous Pillar Array Columns. *Anal. Chem.* **2007**, *79*, 5915−5926.

(11) Mery, E.; Ricoul, F.; Sarrut, N.; Constantin, O.; Delapierre, G.; Garin, J.; Vinet, F. A Silicon Microfluidic Chip Integrating an Ordered Micropillar Array Separation Column and a Nano-Electrospray Emitter for LC/MS Analysis of Peptides. *Sens. Actuators, B* **2008**, *134*, 438−446.

(12) Chan, Y. C.; Zohar, Y.; Lee, Y.-K. Effects of Embedded Sub-Micron Pillar Arrays in Microfluidic Channels on Large DNA Electrophoresis. *Electrophoresis* **2009**, *30*, 3242−3249.

(13) Quéré, D. Wetting and Roughness. *Annu. Rev. Mater. Res.* **2008**, *38*, 71−99.

(14) Diercks, A. H.; Ozinsky, A.; Hansen, C. L.; Spotts, J. M.; David, J. R.; Aderem, A. A Microfluidic Device for Multiplexed Protien Detection in Nano-Liter Volumes. *Anal. Biochem.* **2008**, *2009*, 30−35.

(15) Chin, C.; Laksanasopin, T.; Cheung, Y.; Steinmiller, D.; Linder, V.; Parsa, H.; Wang, J.; Moore, H.; Rouser, R.; Umiviligihozo, G.; Katrita, E.; Mwambarangwe, L.; Braustien, S.; Wijgert, J.; Sahabo, R.; Justman, J.; El-Sadr, W.; Sia, S. Microfluidics-Based Diagnostics of Infectious Diseases in the Developing World. *Nat. Med.* **2011**, *17*, 1015−1019, DOI: 10.1038/nm.2408.

(16) Zhang, F.; Turgeon, N.; Toulouse, M.; Duchaine, C.; Li, D. A Simple and Rapid Fluorescent Neuraminindase Enzymatic Assay on a Microfluidic Chip. *Diagn. Microbiol. Infect. Dis.* **2012**, *74*, 263−6.

(17) Green, J.; Sun, D.; Hafezi-Moghadam, A.; Lashkari, K.; Murthy, S. Microfluidic Pillar Array Sandwich Immunofluorescence Assay for Ocular Diagnostics. *Biomed. Microdevices.* **2011**, *13*, 573−83.

(18) Posthuma-Trumpie, G. A.; Korf, J.; van Amerongen, A. Lateral Flow (Immuno) Assay: Its Strengths, Weaknesses, Opportunities and

Threats. A Literature Survey. *Anal. Bioanal. Chem.* **2009**, *393*, 569−582.
(19) Chu, K.-H.; Xiao, R.; Wang, E. N. Uni-Directional Liquid Spreading on Asymmetric Nanostructured Surfaces. *Nat. Mater.* **2010**, *9*, 413−417.
(20) Xia, D.; Johnson, L. M.; López, G. P. Anisotropic Wetting Surfaces with One-Dimesional and Directional Structures: Fabrication Approaches, Wetting Properties and Potential Applications. *Adv. Mater.* **2012**, *24*, 1287−1302.
(21) Vorobyev, A. Y.; Guo, C. Laser Turns Silicon Superwicking. *Opt. Express* **2010**, *18*, 6455−6460.
(22) Vorobyev, A. Y.; Guo, C. Metal Pumps Liquid Uphill. *Appl. Phys. Lett.* **2009**, *94*, No. 224102.
(23) Callies, M.; Chen, Y.; Marty, F.; Pépin, A.; Quéré, D. Microfabricated Textured Surfaces for Super-Hydrophobicity Investigations. *Microelectron. Eng.* **2005**, *79*, 100−105.
(24) Chen, Y.; Melvin, L. S.; Rodriguez, S.; Bell, D.; Weislogel, M. M. Capillary Driven Flow in Micro Scale Surface Structures. *Microelectron. Eng.* **2009**, *86*, 1317−1320.
(25) Courbin, L.; Denieul, E.; Dressaire, E.; Roper, M.; Ajdari, A.; Stone, H. A. Imbibition by Polygonal Spreading on Microdecorated Surfaces. *Nat. Mater.* **2007**, *6*, 661−664.
(26) Ding, C.; Bogorzi, Srivastava, N.; Sigurdson, M.; Meinhart, C.; MacDonald, N. Super Wetting of Micro and Nano Structured Titania Surfaces. Presented at the 15th International Conference on Solid-State Sensors, Actuators and Microsystems: Transducers 2009, Denver, Colorado, U.S.A., June 21−25, 2009.
(27) Jokinen, V.; Franssila, S. Capillarity in Microfluidic Channels with Hydrophilic and Hydrophobic Walls. *Microfluid. Nanofluid.* **2008**, *5*, 443−448.
(28) Kim, T.-Y.; Ingmar, B.; Bewilogua, K.; Oh, K. H.; Lee, K.-R. Wetting Behaviours of a-C:H:Si:O Film Coated Nano-Scale Dual Rough Surface. *Chem. Phys. Lett.* **2007**, *436*, 199−203.
(29) Rafiee, J.; Rafiee, M. A.; Yu, Z.-Z.; Koratkar, N. Superhydrophobic to Superhydrophilic Wetting Control in Graphene Films. *Adv. Mater.* **2010**, *22*, 2151−2154.
(30) Wang, M.-F.; Raghunathan, N.; Ziaie, B. A Nonlithographic Top−Down Electrochemical Approach for Creating Hierarchical (Micro−Nano) Superhydrophobic Silicon Surfaces. *Langmuir* **2007**, *23*, 2300−2303.
(31) Xiao, R.; Enright, R.; Wang, E. N. Prediction and Optimization of Liquid Propagation in Micropillar Arrays. *Langmuir* **2010**, *26*, 15070−15075.
(32) Wong, T.-S.; Kang, S. H.; Tang, S. K.; Smythe, E. J.; Hatton, B. D.; Grinthal, A.; Aizenberg, J. Bioinspired Self-Repairing Slippery Surfaces with Pressure-Stable Omniphobicity. *Nature* **2011**, *477*, 443−447.
(33) Ishino, C.; Reyssat, M.; Reyssat, E.; Okumura, K.; Quéré, D. Wicking Within Forests of Micropillars. *Europhys. Lett.* **2007**, *79*, No. 56005.
(34) Suzuki, Y.; Yokoyama, K. Construction of a More Sensitive Fluorescence Sensing Material for the Detection of Vascular Endothelial Growth Factor, A Biomarker for Angiogenesis, Prepared by Combining a Fluorescent Peptide and a Nanopillar Substrate. *Biosens. Bioelectron.* **2011**, *26*, 3696−3699.
(35) Mai, T. T.; Lai, C. Q.; Zheng, H.; Balasubramanian, K.; Leong, K. C.; Lee, P. S.; Lee, C.; Choi, W. K. Dynamics of Wicking in Silicon Nanopillars Fabricated with Interference Lithography and Metal-Assisted Chemical Etching. *Langmuir* **2012**, *28*, 11465−11471.
(36) Huang, Z.; Fang, H.; Zhu, J. Fabrication of Silicon Nanowire Arrays with Controlled Diameter, Length, and Density. *Adv. Mater.* **2007**, *19*, 744−748.
(37) Hsu, C.-M.; Connor, S. T.; Tang, M. X.; Cui, Y. Wafer-Scale Silicon Nanopillars and Nanocones by Langmuir−Blodgett Assembly and Etching. *Appl. Phys. Lett.* **2008**, *93*, No. 133109.
(38) Reijnders, L. Cleaner Nanotechnology and Hazard Reduction of Manufactured Nanoparticles. *J. Cleaner Prod.* **2006**, *14*, 124−133.
(39) Agapov, R.; Bernadeta, S.; Chris, F.; Dayrl, B.; Nickolay, V. L.; Michael, J. S. Lithography-Free Approach to Highly Efficient, Scalable SERS Substrates Based on Disordered Clusters of Disc-on-Pillar Structures. *Nanotechnology* **2013**, *24*, 505302.
(40) Batey, J.; Tierney, E. Low-Temperature Deposition of High-Quality Silicon Dioxide by Plasma-Enhanced Chemical Vapor Deposition. *J. Appl. Phys.* **1986**, *60*, 3136−3145.
(41) Ceiler, M.; Kohl, P.; Bidstrup, S. Plasma-Enhanced Chemical Vapor Deposition of Silicon Dioxide Deposited at Low Temperatures. *J. Electrochem. Soc.* **1995**, *142*, 2067−2071.
(42) Borrás, A.; Barranco, A.; González-Elipe, A. R. Design and Control of Porosity in Oxide Thin Films Grown by PECVD. *J. Mater. Sci.* **2006**, *41*, 5220−5226.
(43) Wang, D.; Ji, R.; Schaaf, P. Formation of Precise 2D Au Particle Arrays Via Thermally Induced Dewetting on Pre-Patterened Substrates. *Beilstein J. Nanotechnol.* **2011**, *2*, 318−326.
(44) Bico, J.; Tordeux, C.; Quéré, D. Rough Wetting. *Europhys. Lett.* **2001**, *55*, 214.
(45) Lee, J.-M.; Kim, B.-I. Thermal Dewetting of Pt Thin Film: Etch-Masks for the Fabrication of Semiconductor Nanostructures. *Mater. Sci. Eng.: A* **2007**, *449*, 769−773.
(46) Agapov, R. L.; Boreyko, J. B.; Briggs, D. P.; Srijanto, B. R.; Retterer, S. T.; Collier, C. P.; Lavrik, N. V. Asymmetric Wettability of Nanostructures Directs Leidenfrost Droplets. *ACS Nano* **2013**, *8*, 860−867.
(47) Reynolds, O. An Experimental Investigation of the Circumstances which Determine Whether the Motion of Water Shall be Direct or Sinuous, and of the Law of Resistance in Parallel Channels. *Proc. R. Soc. London* **1883**, *35*, 84−99.
(48) Murakami, D.; Jinnai, H.; Takahara, A. Wetting Transition from the Cassie−Baxter State to the Wenzel Stateon Textured Polymer Surfaces. *Langmuir* **2014**, *30*, 2061−6067.
(49) Kang, S.; Hwang, S.; Jin, S.; Choi, C.; Kim, J.; Park, B. A Rapid One-Step Fabrication of Patternable Superhydrophobic Surfaces Driven by Marangoni Instability. *Langmuir* **2014**, *30*, 2828−2834.